Analytica Chimica Acta 1206 (2022) 339648

Contents lists available at ScienceDirect

Analytica Chimica Acta

journal homepage: www.elsevier.com/locate/aca

Electrochemiluminescence enhanced by isolating ACQphores in pyrene-based porous organic polymer: A novel ECL emitter for the construction of biosensing platform

Yong-Jiang Zhang , Yang Yang , Jun-Mao Wang , Wen-Bin Liang , Ruo Yuan , Dong-Rong Xiao *

Key Laboratory of Luminescence Analysis and Molecular Sensing of Ministry of Education, College of Chemistry and Chemical Engineering, Southwest University, Chongqing, 400715, PR China

HIGHLIGHTS

- Py-POP was synthesized to construct biosensors for the ultrasensitive detection of miRNA-155.
- The Py-POP's skeleton could isolate ACQphores with each other, which suppressed ACQ effect and enhanced the ECL emission.
- Py-POP was synthesized by ECL-active monomers, which increased the loading number of ECL luminophores.

GRAPHICAL ABSTRACT

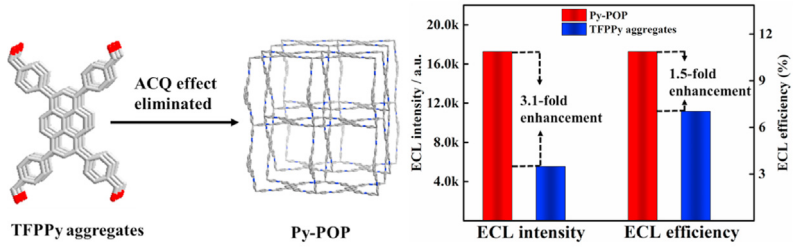

ARTICLE INFO

Article history:
Received 10 December 2021
Received in revised form
31 January 2022
Accepted 22 February 2022
Available online 24 February 2022

Keywords:
Porous organic polymer
ECL biosensor
Isolation of ACQphores
Elimination of ACQ effect
MicroRNA-155

ABSTRACT

In this work, a pyrene-based porous organic polymer (Py-POP) with strong electrochemiluminescence (ECL) emission was synthesized and used to fabricate an ECL sensor for the extra-sensitive detection of microRNA-155. The ECL intensity of the Py-POP prepared by tetra(*p*-aminophenyl)methane (TAPM) and 1,3,6,8-tetrakis(4-formylphenyl)pyrene (TFPPy) was about 3.1 times that of TFPPy aggregates, which was primarily ascribed to the elimination of the effect of aggregation-caused quenching (ACQ) by increasing the distance between ACQ luminophores (pyrene cores) in Py-POP. Meanwhile, the strong covalent connections between 1,3,6,8-tetraphenylpyrene (TPPy) and tetraphenylmethane (TPM) units in the rigid framework of Py-POP could partly block the intramolecular motion of TPPy and TPM, which reduced the non-radiative decay and thus further improved the ECL emission. Furthermore, the hydrophobic porous structure of Py-POP was beneficial to the enrichment of lipophilic tripropylamine (TPrA) coreactants in pores of Py-POP, which greatly shortened the electron migration distance between TPrA coreactants and pyrene luminophores on the pore walls of Py-POP, thereby also enhancing the ECL intensity. By using the Py-POP as a new ECL tag and with the help of the strand displacement processes and target recycling, the fabricated ECL biosensor had a sensitive response for microRNA-155 from 1 fM to 1 nM and a detection limit of 0.326 fM. Overall, this work provided a new and feasible strategy to surmount the ACQ effect for enhancing ECL emission, which not only paved a new way to exploit high-performance ECL materials for fabricating extra-sensitive sensors but also broadened the application of POPs in bioanalysis and ECL fields.

© 2022 Elsevier B.V. All rights reserved.

* Corresponding author.
E-mail address: xiaodr98@swu.edu.cn (D.-R. Xiao).

https://doi.org/10.1016/j.aca.2022.339648
0003-2670/© 2022 Elsevier B.V. All rights reserved.

1. Introduction

Electrochemiluminescence (ECL) is one of the most popular methods for bioanalysis owing to its low background, high sensitivity, excellent controllability, and inexpensive cost [1–3]. Because the concentration of cancer biomarkers is very low in the early stage which can not be detected by clinical diagnosis [4,5], developing the extra-sensitive ECL biosensor for early diagnosis of cancer is necessary. One of the most feasible ways of improving the sensitivity of ECL biosensors is enhancing the loading number of luminophores to obtain high-performance ECL materials [6–8]. Recently, many materials as carriers employed to load ECL luminophores have been reported, such as carbon nanotubes [9], silica nanoparticles [10], and metal-organic frameworks (MOFs) [11–13]. In these carrier materials, MOFs have received considerable research enthusiasm because of the ultrahigh surface area and ordered porosity [14], which could largely improve the immobilization number of ECL luminophores [15]. However, because most MOFs are not stable in water, the decomposition of MOFs will cause the leakage of luminophores during the experiment process [16], which would influence the reproducibility and stability of MOF-based ECL biosensors. Hence, it is imperative to design and synthesize new porous ECL materials with a large immobilization number of luminophores and better water stability for fabricating ultrasensitive ECL biosensors.

Porous organic polymers (POPs), synthesized from organic monomers via robust covalent connections, including covalent organic frameworks, conjugated microporous polymers, and porous aromatic frameworks, are a new type of porous materials with better water stability than MOFs [3,17–22]. More importantly, POPs can be synthesized from ECL-active organic monomers directly, which may largely enhance the loading number of ECL luminophores [3]. Although POPs have these advantages, there are just a few works reported about POPs applied in ECL fields. The reason may be that the ECL emission of POPs is easily weakened or annihilated by the effect of aggregation-caused quenching (ACQ) that results from π-π stacking between aromatic rings [23]. Recently, Tang's group has converted the ACQ luminophores (ACQphores) to aggregation-induced emission (AIE) luminogens via connecting AIE molecules with planar ACQphores [24], which broke the molecular planarity by the twisted AIE molecules, and thus impeded detrimental π-π stacking to eliminate ACQ effect. Inspired by the above research, we speculate that ECL-active POPs may be designed by connecting planar ACQphores with tetrahedral monomers, which can isolate ACQphores with each other and thus overcome the ACQ effect to achieve ECL enhancement. With this in mind, we used tetra(*p*-aminophenyl)methane (TAPM) to react with 1,3,6,8-tetrakis(4-formylphenyl)pyrene (TFPPy, Scheme 1A) and successfully synthesized an ECL-active Py-POP. Gratifyingly, the ECL intensity and ECL efficiency of Py-POP were respectively about 3.1 times and 1.5 times those of TFPPy aggregates at the same conditions. The excellent ECL performance of Py-POP might be due to four reasons. (1) The ACQphores (pyrene cores) were isolated with each other in the rigid skeleton of Py-POP, which suppressed the π-π stacking between pyrene rings and thus surmounted the ACQ effect. (2) The loading amount of ECL luminophores (pyrene cores) was largely increased because TFPPy was employed as monomers to synthesize Py-POP. (3) In the Py-POP, the 1,3,6,8-tetraphenylpyrene (TPPy) and tetraphenylmethane (TPM) units were stretched and fixed by covalent connections from four different directions (Scheme 1A and Fig. S1), which could impede intramolecular motions of TPPy and TPM to some extent [25], thereby diminishing the non-radiative energy loss. (4) The hydrophobicity of Py-POP was beneficial to the concentration and enrichment of lipophilic tripropylamine (TPrA) co-reactants in the pores of Py-POP, thus effectively shortening the electron transfer path between TPrA co-reactants and pyrene luminophores. All these features were helpful to improve the ECL performance of Py-POP.

MicroRNA-155 (miRNA-155) was associated with a series of diseases such as asthma, atherosclerosis and cervical cancer [26–28], hence it was meaningful to detect miRNA-155 sensitively. On account of the excellent ECL property of Py-POP, we constructed an ultrasensitive ECL biosensor for miRNA-155 detection by utilizing Py-POP as a new ECL probe combined with the strand displacement amplification (SDA) and target cycling strategies. Scheme 1B displayed the fabrication procedure of the ECL biosensor. Firstly, Py-POP was dropped onto the bare electrode. After Py-POP formed a film on the electrode, the Au nanoparticles (AuNPs) were modified on the film. Next, the capture probe (CP) was fixed onto the AuNPs, and the hexanethiol (HT) was subsequently used for blocking the nonspecific sites. Then, CP hybridized with the ferrocene-labeled DNA (S1-Fc), which could make the ECL signal of Py-POP quench (signal-off). The target cycling and SDA strategies were shown in Scheme 1C. MiRNA-155 as the target could hybridize with hairpin DNA (H1) to form the miRNA-155-H1 complex, which was subsequently hybridized with primer. Aiding by deoxyribonucleoside triphosphates (dNTPs) and phi29 polymerase, the primer could be extended along the H1 template to produce double-stranded DNA (dsDNA) and release miRNA-155 for the next cycle (cycle I). The dsDNA could be cleaved by Nb.BbvCI, and the target substitute (output S2) was released by the polymerization reaction of phi29. Meanwhile, dsDNA was gained again. After the continuous cycling reactions of cleaving and polymerization (cycle II), plenty of output S2 was released and then used to displace S1-Fc hybridized with CP, leading to the detachment of S1-Fc, so the ECL signal recovered (signal-on). Gratifyingly, the Py-POP-based ECL biosensor realized the extra-sensitive measurement of miRNA-155. Significantly, the finding of isolating ACQphores in POPs for ECL enhancement provided a novel conception for designing ECL materials with excellent properties, thus revealing a new avenue to exploit extra-sensitive ECL biosensors, which expanded the application scope of POPs.

2. Experimental procedure

2.1. Materials and reagents and Synthesis of Py-POP

Materials and reagents, the synthesis of Py-POP, were shown in supporting information.

2.2. Fabrication of the ECL sensor

Firstly, the glassy carbon electrode (GCE) was burnished with 0.3 and 0.05 μm of Al_2O_3 powder respectively. Secondly, dropped the Py-POP (0.5 mg/mL, 10 μL) on the GCE to form a film at 37 °C. Thirdly, 10 μL of AuNPs was decorated on the Py-POP film, and the capture probe (CP, 0.5 μM, 10 μL) was modified onto the electrode at 4 °C for 10 h after the AuNPs solution dried. Then, 10 μL of HT (in ethanol, 1 mM) was incubated onto the electrode for 40 min to block the non-specific sites. After that, added S1-Fc (2 μM, 10 μL) to the electrode for 3 h. Lastly, a 10 μL product of the target cycling and SDA reaction was incubated onto the electrode at 37 °C for 2 h. It is

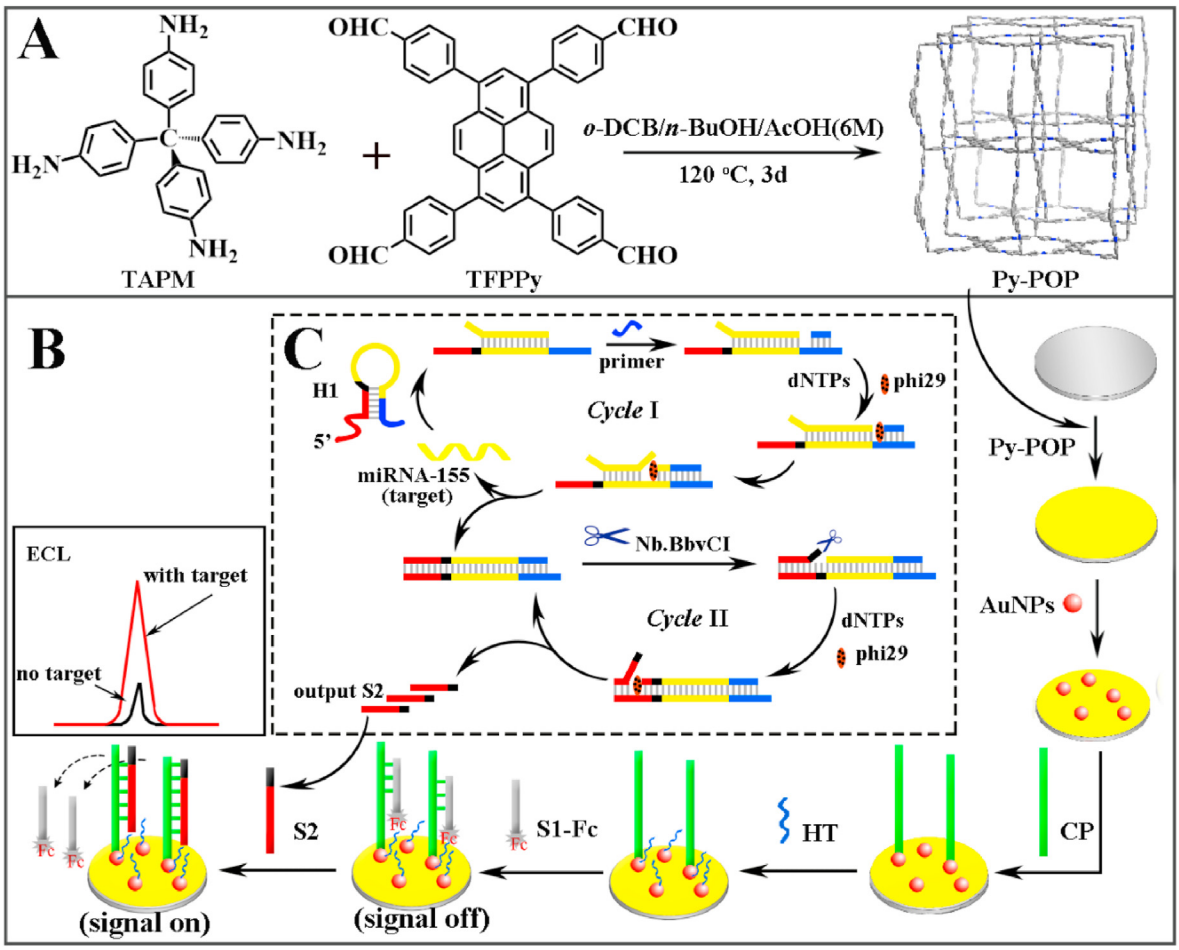

Scheme 1. (A) Synthesis of Py-POP. (B) Construction process of ECL biosensor. (C) The target recycling and SDA strategies.

noteworthy that every modification needs to be rinsed with ultrapure water for removing the remaining reagents. The characterization of the ECL sensor was placed in S9.

2.3. Measurement procedure

To detect miRNA-155, the ECL responses were measured in 2 mL PBS (0.1 M, PH 7.4) including 10 μL of TPrA with a potential scanning from 0.4 to 1.6 V (scanning speed: 0.2 V/s). The photomultiplier voltage was 800 V.

3. Results and discussion

3.1. Characterization of Py-POP

The scanning electron microscopy (SEM) images (Fig. 1A) indicated that Py-POP exhibited a granular shape with a diameter of about 1 μm. The FT-IR spectra of TFPPy and Py-POP were displayed in Fig. 1B. The band at 1699 cm^{-1} in TFPPy was C=O stretching peak which diminished absolutely in FT-IR spectrum of Py-POP. The new band at 1621 cm^{-1} of Py-POP was C=N stretching peak, which proved the formation of imine linkages in Py-POP. Thermogravimetric analysis (TGA) showed the first weight loss of degassed Py-POP after 275 °C (Fig. 1C), which indicated that the Py-POP was thermally stable at temperature up to 275 °C.

The porosity of Py-POP was investigated by nitrogen adsorption measurement at 77 K. The isotherm (Fig. 2A) displayed a very sharp uptake when the relative pressure (P/P_0) was less than 0.1, which meant the existence of micropores. The Brunauer-Emmett-Teller surface area and pore volume were respectively calculated as 125 $m^2\ g^{-1}$ and 0.13 $cm^3\ g^{-1}$. The pore size distribution of Py-POP exhibited a major peak centered at 1.30 nm (Fig. 2B).

3.2. Luminescence properties of Py-POP

The luminescent characteristics of Py-POP were investigated by ECL and photoluminescence (PL) spectra. The ECL-wavelength-potential 3D color map (Fig. 3A) and ECL heat map image (Fig. 3B) of Py-POP were acquired under a scanning potential of 0.4–1.6 V, which intuitively displayed the maximum ECL emission at 495 nm. The maximum PL emission peak in Fig. 3C was about 500 nm, which was almost the same place as the maximum ECL emission peak.

3.3. ECL performance of Py-POP

The ECL performance of Py-POP was compared with TFPPy aggregates (Fig. 4A). The average ECL intensity of Py-POP (red curve) was 16912 a.u., which was about 3.1 times that of TFPPy aggregates (Fig. 4A, blue curve, 5540 a.u.) under the same test condition. The related current signals were shown in Fig. 4B. Furthermore, according to the ECL efficiency (Φ_{ECL}) of $[Ru(bpy)_3]^{2+}$ system (5%) as reference, the Φ_{ECL} of Py-POP/TPrA system was calculated as 10.87%, which was about 1.5 times that of TFPPy aggregates/TPrA system

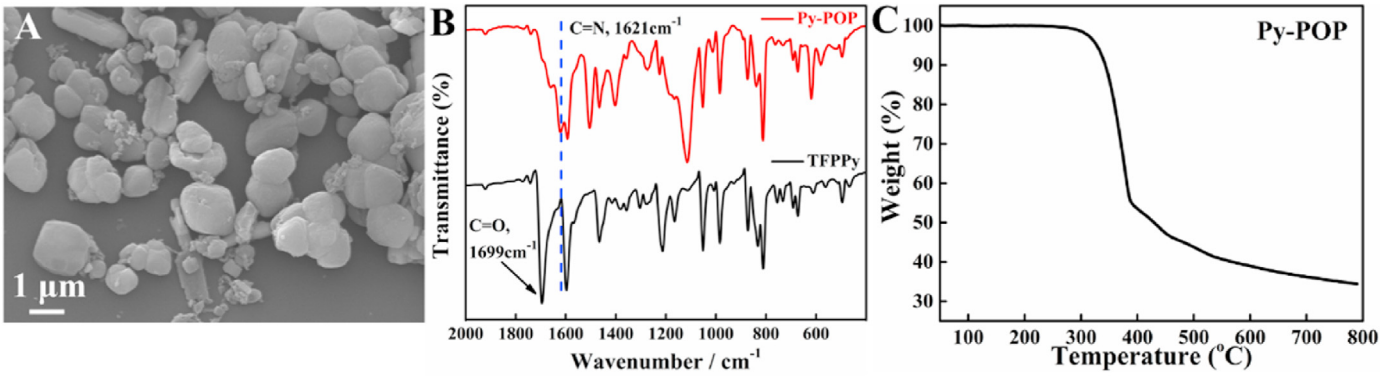

Fig. 1. (A) SEM image of Py-POP. (B) FT-IR spectra of Py-POP and TFPPy. (C) TGA of degassed Py-POP.

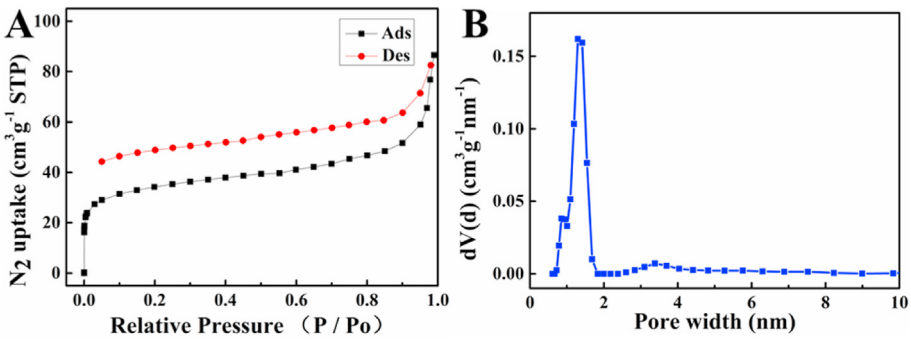

Fig. 2. (A) Nitrogen adsorption-desorption isotherms of Py-POP. (B) Pore size distribution of Py-POP.

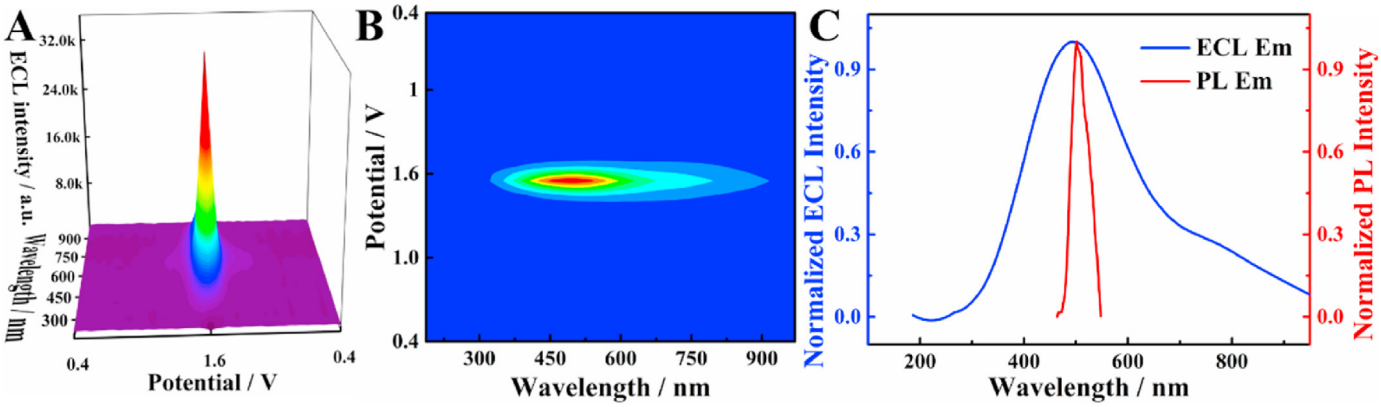

Fig. 3. (A) 3D color map surface and (B) Heat map image of ECL from Py-POP (0.5 mg/mL, 10 μL) tested in 2 mL PBS (0.1 M, pH 7.4) containing 10 μL TPrA. (C) Normalized ECL emission spectrum and PL emission spectrum of Py-POP. (For interpretation of the references to color in this figure legend, the reader is referred to the Web version of this article.)

(Φ_{ECL} = 7.09%, Table S2). Hence, it was a feasible strategy to enhance ECL intensity and efficiency by isolating ACQphores in POPs to overcome the ACQ effect.

3.4. Possible ECL mechanism of the ECL sensor

The cyclic voltammetry (CV) and ECL responses were measured to explore the possible ECL mechanism (Fig. 5). The bare GCE (Fig. 5A a and Fig. 5B a) showed no redox peaks and no ECL signal in PBS. When TPrA was added in the PBS, an oxidation peak at 0.93 V was observed in Fig. 5A b, and the related ECL signal was about 60 a.u. (Fig. 5B b). As depicted in Fig. 5A c, Py-POP modified GCE (Py-POP/GCE) revealed an oxidation peak at 1.37 V in the absence of TPrA, and the relevant ECL intensity was approximate 110 a.u. (Fig. 5B c). However, in the presence of TPrA, Py-POP/GCE exhibited an obvious shift of the oxidation potential from 1.37 V to 1.06 V and had a higher peak current (Fig. 5A d). At the same time, the corresponding ECL signal rose significantly and reached 16459 a.u. (Fig. 5B d). These results indicated that TPrA acted as a co-reactant to enhance the ECL signal of Py-POP, and the possible ECL mechanism was as follows.

$$Py - POP - e^{-} \rightarrow Py - POP^{+} \quad (1)$$

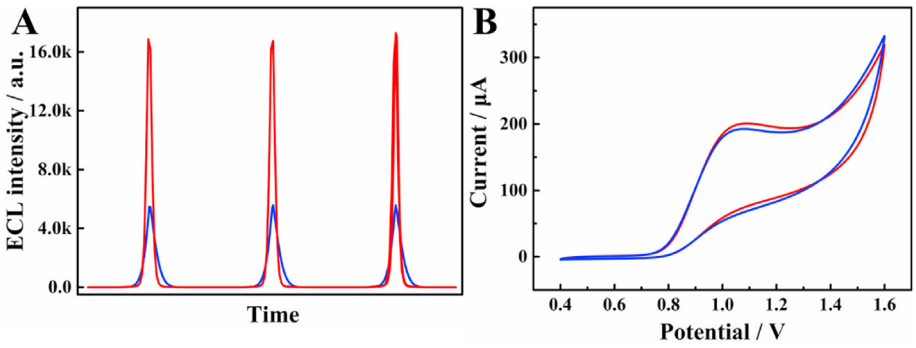

Fig. 4. (A) ECL intensities, (B) Current signals of Py-POP/GCE (0.5 mg/mL, 10 μL, red curve) and TFPPy aggregates/GCE (0.5 mg/mL, 10 μL, blue curve) in 2 mL PBS (0.1 M, pH 7.4) containing 10 μL of TPrA. (For interpretation of the references to color in this figure legend, the reader is referred to the Web version of this article.)

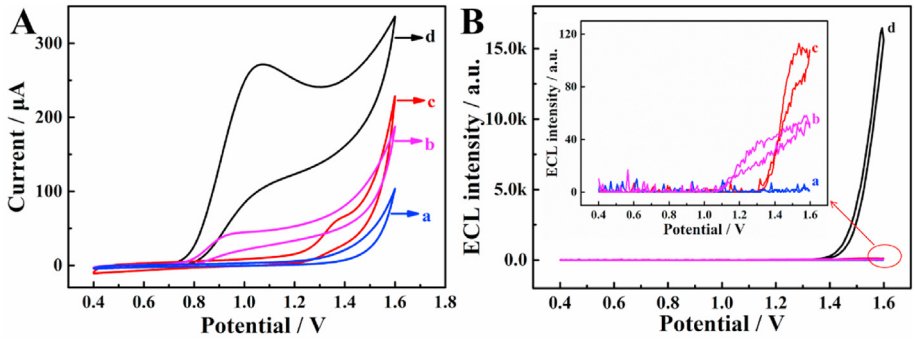

Fig. 5. (A) CV and (B) ECL curves of different modified electrodes: (a) bare GCE and (c) Py-POP/GCE (0.5 mg/mL, 10 μL) in 2 mL PBS (0.1 M, pH 7.4), (b) bare GCE and (d) Py-POP/GCE (0.5 mg/mL, 10 μL) in 2 mL PBS (0.1 M, pH 7.4) containing 10 μL TPrA.

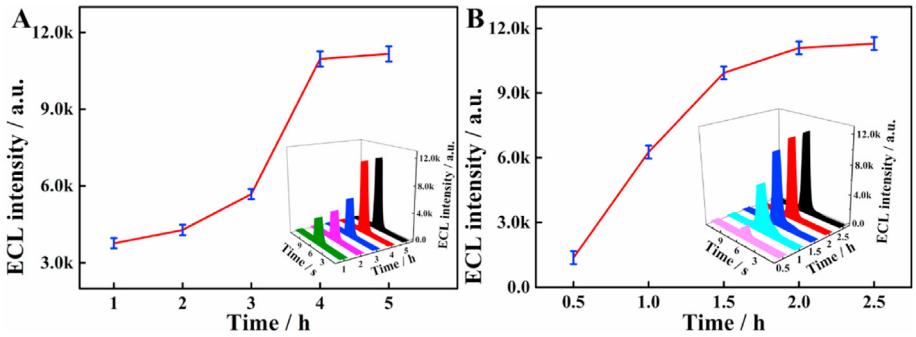

Fig. 6. Optimization of the experimental conditions ($c_{miRNA\text{-}155}$ = 10 pM): (A) the SDA reaction time, (B) the incubation time of output S2 modified on the S1-Fc/HT/CP/AuNPs/Py-POP/GCE.

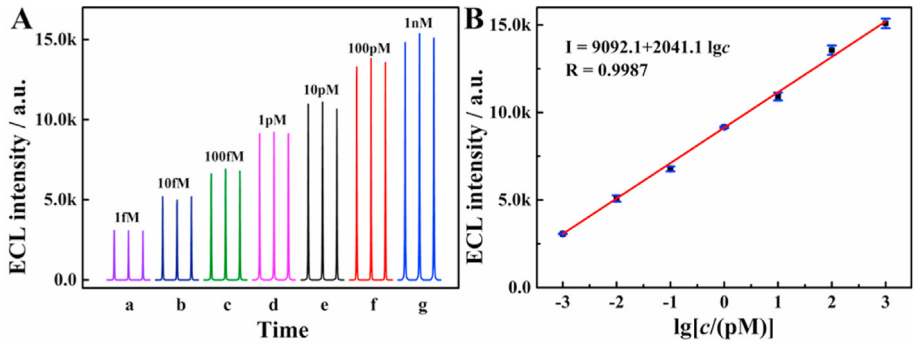

Fig. 7. (A) ECL responses towards different miRNA-155 concentrations. (B) Linear correlation plot for miRNA-155 detection.

Table 1
Comparison of Different Methods for miRNA-155 Detection.

Method	Linear range	LOD	Ref.
Electrochemistry	10 fM – 10 nM	10 fM	[29]
Fluorescence	1.56 fM – 5 nM	1.33 fM	[30]
Fluorescence	0.1 nM – 200 nM	100 pM	[31]
Fluorescence	5 pM – 10 nM	2.2 pM	[32]
ECL	10 fM – 10 nM	2.7 fM	[33]
ECL	1 pM – 10 μM	0.67 pM	[34]
ECL	10 fM – 100 nM	5.7 fM	[35]
ECL	1 fM – 1 nM	0.326 fM	This work

$$TPrA - e^{-} \rightarrow TPrA^{\bullet +} \quad (2)$$

$$TPrA^{\bullet +} \rightarrow TPrA^{\bullet} + H^{+} \quad (3)$$

$$Py - POP^{+} + TPrA^{\bullet} \rightarrow Py - POP^{*} + products \quad (4)$$

$$Py - POP^{*} \rightarrow Py - POP + h\nu \quad (5)$$

3.5. Optimization of the experimental conditions

SDA reaction time was optimized to acquire the optimum properties of the as-prepared ECL sensor. As the increase of SDA reaction time, the ECL signal progressively enhanced and tended to be a platform at 4 h (Fig. 6A). Hence, 4 h was chosen for the SDA reaction time. In addition, the incubation time of output S2 modified on S1-Fc/HT/CP/AuNPs/Py-POP/GCE was also optimized. The ECL intensity (Fig. 6B) enhanced continuously with the incubation time and became stabilized at 2 h, so 2 h was the optimal incubation time of output S2 modified on the electrode.

3.6. Detection of miRNA-155 with the ECL sensor

The sensitivity of the developed ECL sensor was assessed via detecting miRNA-155 of various concentrations. The ECL intensity (Fig. 7A) was enhanced with the increasing miRNA-155 concentrations (1 fM-1 nM). Moreover, it was found from Fig. 7A that the ECL signals (I) linearly increased with the logarithm of miRNA-155 concentrations (c). And the relative linear regression equation was $I = 9092.1 + 2041.1 \lg[c/(\mathrm{pM})]$ with a correlation coefficient of 0.9987 and a detection limit of 0.326 fM (calculation was shown in S10). Additionally, in comparison with some previous methods (Table 1), the proposed ECL sensor had a lower detection limit.

3.7. Stability, selectivity, and reproducibility of the ECL sensor

Stability, reproducibility, and selectivity were vital factors to assess the practicability of the ECL sensor. As shown in Fig. 8A, the ECL biosensor displayed steady signals during a continuous scan of 24 cycles (100 fM miRNA-155) with relative standard deviations (RSD) of 2.60%, proving the well stability of the ECL biosensor. Moreover, to investigate the selectivity of the ECL biosensor, miRNA-21 (100 pM), miRNA-141 (100 pM), thrombin aptamer (TBA, 100 pM) and miRNA-199a (100 pM) were employed as interferences. As observed in Fig. 8B, the ECL responses of these interferences were similar to the blank sample. Furthermore, the ECL response of the mixture (10 pM miRNA-155, 100 pM miRNA-21, 100 pM miRNA-141, 100 pM miRNA-199a and 100 pM TBA) was approximately the same as that of target miRNA-155 (10 pM). These results indicated that the fabricated biosensor exhibited distinguished selectivity for detecting miRNA-155. In addition, the reproducibility was evaluated by testing inter-assays of five electrodes at 100 fM miRNA-155, and the RSD value was 2.67% (Fig. 8C), which illustrated the constructed ECL biosensor had acceptable reproducibility.

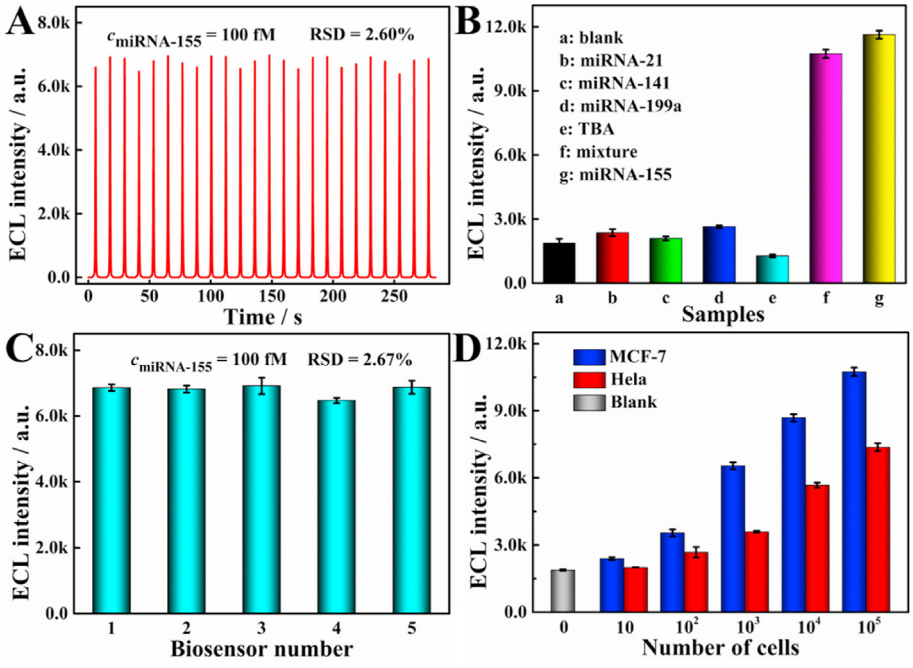

Fig. 8. (A) Stability of the constructed biosensor. (B) Selectivity of the biosensor for various targets. (C) Reproducibility of the fabricated biosensor. (D) ECL analysis of the biosensor for miRNA-155 in MCF-7 and HeLa cells.

3.8. Application

The lysates of HeLa and MCF-7 cells were employed to examine the preliminary practicability of the sensing platform in real samples. The ECL responses (Fig. 8D) were enhanced with the increasing cell numbers from 0 to 10^5, while the ECL response of MCF-7 enhanced more obviously than that of HeLa. Such results revealed that the expression of miRNA-155 in HeLa was lower than that in MCF-7, which agreed with the previous reports [36,37]. Therefore, the fabricated ECL biosensor was preliminarily practicable to detect miRNA-155 in cancer cells.

4. Conclusions

In summary, in order to surmount the ACQ effect for ECL enhancement, we have rationally designed and synthesized an ECL-active Py-POP by condensation of TFPPy with TAPM, which isolated ACQphores (pyrene cores) with each other, reduced the non-radiative decay via restricting the intramolecular motions of TPPy and TPM, and shortened electron transfer path between TPrA co-reactants and pyrene luminophores through enrichment of lipophilic TPrA in the pores. As a result, the ECL efficiency and intensity of the Py-POP were about 1.5 times and 3.1 times those of TFPPy aggregates, respectively. By employing the Py-POP as a high-efficiency ECL tag, the constructed ECL sensor successfully achieved the sensitive detection of miRNA-155. In brief, this work provided an efficient strategy to enhance ECL emission by solving the ACQ problem, which provided a novel idea to devise highly efficient POP-based ECL emitters, thereby opening a new chapter to exploit new kinds of ECL materials for constructing ultrasensitive ECL sensors.

CRediT authorship contribution statement

Yong-Jiang Zhang: Conceptualization, Data curation, Formal analysis, Investigation, Writing – original draft. **Yang Yang:** Investigation, Data curation, Formal analysis. **Jun-Mao Wang:** Data curation, Investigation. **Wen-Bin Liang:** Data curation, Writing – review & editing. **Ruo Yuan:** Conceptualization, Resources. **Dong-Rong Xiao:** Conceptualization, Project administration, Funding acquisition, Resources, Writing – review & editing, Supervision.

Declaration of competing interest

The authors declare that they have no known competing financial interests or personal relationships that could have appeared to influence the work reported in this paper.

Acknowledgments

This work was financially supported by the NSFC (21571149), and Chongqing Overseas Returnees Innovation Program (cx2017007, cx2018026).

Appendix A. Supplementary data

Supplementary data to this article can be found online at https://doi.org/10.1016/j.aca.2022.339648.

References

[1] Z. Xu, Y. Chang, Y. Chai, H. Wang, R. Yuan, Ultrasensitive electrochemiluminescence biosensor for speedy detection of microRNA based on a DNA rolling machine and target recycling, Anal. Chem. 91 (2019) 4883–4888.
[2] Z. Liu, W. Qi, G. Xu, Recent advances in electrochemiluminescence, Chem. Soc. Rev. 44 (2015) 3117–3142.
[3] J.-L. Zhang, Y. Yang, W.-B. Liang, L.-Y. Yao, R. Yuan, D.-R. Xiao, Highly stable covalent organic framework nanosheets as a new generation of electrochemiluminescence emitters for ultrasensitive microRNA detection, Anal. Chem. 93 (2021) 3258–3265.
[4] A.R. Cardoso, F.T.C. Moreira, R. Fernandes, M.G.F. Sales, Novel and simple electrochemical biosensor monitoring attomolar levels of miRNA-155 in breast cancer, Biosens. Bioelectron. 80 (2016) 621–630.
[5] H. Dong, J. Lei, L. Ding, Y. Wen, H. Ju, X. Zhang, MicroRNA: function, detection, and bioanalysis, Chem. Rev. 113 (2013) 6207–6233.
[6] G.-B. Hu, C.-Y. Xiong, W.-B. Liang, Y. Yang, L.-Y. Yao, W. Huang, et al., Highly stable Ru-complex-grafted 2D metal-organic layer with superior electrochemiluminescent efficiency as a sensing platform for simple and ultrasensitive detection of mucin 1, Biosens. Bioelectron. 135 (2019) 95–101.
[7] L.-Y. Yao, F. Yang, W.-B. Liang, G.-B. Hu, Y. Yang, W. Huang, et al., Ruthenium complex doped metal-organic nanoplate with high electrochemiluminescent intensity and stability for ultrasensitive assay of mucin 1, Sensor. Actuator. B Chem. 292 (2019) 105–110.
[8] Y. Yang, G.-B. Hu, W.-B. Liang, L.-Y. Yao, W. Huang, Y.-J. Zhang, et al., An AIEgen-based 2D ultrathin metal–organic layer as an electrochemiluminescence platform for ultrasensitive biosensing of carcinoembryonic antigen, Nanoscale 12 (2020) 5932–5941.
[9] G. Lai, F. Yan, H. Ju, Dual signal amplification of glucose oxidase-functionalized nanocomposites as a trace label for ultrasensitive simultaneous multiplexed electrochemical detection of tumor markers, Anal. Chem. 81 (2009) 9730–9736.
[10] X. Yang, R. Yuan, Y. Chai, Y. Zhuo, L. Mao, S. Yuan, $Ru(bpy)_3^{2+}$-doped silica nanoparticles labeling for a sandwich-type electrochemiluminescence immunosensor, Biosens. Bioelectron. 25 (2010) 1851–1855.
[11] W. Huang, G.-B. Hu, L.-Y. Yao, Y. Yang, W.-B. Liang, R. Yuan, et al., Matrix coordination-induced electrochemiluminescence enhancement of tetraphenylethylene-based hafnium metal–organic framework: an electrochemiluminescence chromophore for ultrasensitive electrochemiluminescence sensor construction, Anal. Chem. 92 (2020) 3380–3387.
[12] L.-Y. Yao, F. Yang, G.-B. Hu, Y. Yang, W. Huang, W.-B. Liang, et al., Restriction of intramolecular motions (RIM) by metal-organic frameworks for electrochemiluminescence enhancement: 2D Zr_{12}-adb nanoplate as a novel ECL tag for the construction of biosensing platform, Biosens. Bioelectron. 155 (2020), 112099.
[13] Y. Yang, G.-B. Hu, W.-B. Liang, L.-Y. Yao, W. Huang, R. Yuan, et al., A highly sensitive self-enhanced aptasensor based on a stable ultrathin 2D metal–organic layer with outstanding electrochemiluminescence property, Nanoscale 11 (2019) 10056–10063.
[14] J. Zhou, Y. Li, W. Wang, X. Tan, Z. Lu, H. Han, Metal-organic frameworks-based sensitive electrochemiluminescence biosensing, Biosens. Bioelectron. 164 (2020), 112332.
[15] W. Huang, G.-B. Hu, W.-B. Liang, J.-M. Wang, M.-L. Lu, R. Yuan, et al., Ruthenium(II) complex-grafted hollow hierarchical metal–organic frameworks with superior electrochemiluminescence performance for sensitive assay of thrombin, Anal. Chem. 93 (2021) 6239–6245.
[16] G.-B. Hu, C.-Y. Xiong, W.-B. Liang, X.-S. Zeng, H.-L. Xu, Y. Yang, et al., Highly stable mesoporous luminescence-functionalized MOF with excellent electrochemiluminescence property for ultrasensitive immunosensor construction, ACS Appl. Mater. Interfaces 10 (2018) 15913–15919.
[17] A. Trewin, A.I. Cooper, Porous organic polymers: distinction from disorder? Angew. Chem. Int. Ed. 49 (2010) 1533–1535.
[18] Q. Chen, A. Dong, D. Wang, L. Qiu, C. Ma, Y. Yuan, et al., Efficient and selective methane borylation through pore size tuning of hybrid porous organic-polymer-based iridium catalysts, Angew. Chem. Int. Ed. 58 (2019) 10671–10676.
[19] Y. Zhang, S.N. Riduan, Functional porous organic polymers for heterogeneous catalysis, Chem. Soc. Rev. 41 (2012) 2083–2094.
[20] J.W. Powell, R.P. Chartoff, Viscoelastic properties and stability of BBL ladder polymers, J. Appl. Polym. Sci. 18 (1974) 83–91.
[21] S.H. Li, X.H. Ma, C.H. Pang, M.Y. Wang, G.H. Yin, Z. Xu, J.P. Li, J.H. Luo, Novel chloramphenicol sensor based on aggregation-induced electrochemiluminescence and nanozyme amplification, Biosens. Bioelectron. 176 (2021), 112944.
[22] W.-R. Cui, Y.-J. Li, Q.-Q. Jiang, Q. Wu, Q.-X. Luo, L. Zhang, et al., Covalent organic frameworks as advanced uranyl electrochemiluminescence monitoring platforms, Anal. Chem. 93 (2021) 16149–16157.
[23] Q. Gao, X. Li, G.-H. Ning, K. Leng, B. Tian, C. Liu, et al., Highly photoluminescent two-dimensional imine-based covalent organic frameworks for chemical sensing, Chem. Commun. 54 (2018) 2349–2352.
[24] J. Mei, N.L.C. Leung, R.T.K. Kwok, J.W.Y. Lam, B.Z. Tang, Aggregation-induced emission: together we shine, united we soar, Chem. Rev. 115 (2015) 11718–11940.
[25] Y. Xu, L. Chen, Z. Guo, A. Nagai, D. Jiang, Light-emitting conjugated polymers with microporous network architecture: interweaving scaffold promotes electronic conjugation, facilitates exciton migration, and improves luminescence, J. Am. Chem. Soc. 133 (2011) 17622–17625.
[26] Y. Yang, L. Yang, X. Liang, G. Zhu, MicroRNA-155 promotes atherosclerosis inflammation via targeting SOCS1, Cell. Physiol. Biochem. 36 (2015) 1371–1381.
[27] H. Fang, D. Shuang, Z. Yi, H. Sheng, Y. Liu, Up-regulated microRNA-155 expression is associated with poor prognosis in cervical cancer patients,

Biomed. Pharmacother. 83 (2016) 64–69.
[28] E.E. Blomme, S. Provoost, E. Bazzan, H.P. Van Eeckhoutte, M.P. Roffel, L. Pollaris, et al., Innate lymphoid cells in isocyanate-induced asthma: role of microRNA-155, Eur. Respir. J. 56 (2020), 1901289.
[29] D. Zeng, Z. Wang, Z. Meng, P. Wang, L. San, W. Wang, et al., DNA tetrahedral nanostructure-based electrochemical miRNA biosensor for simultaneous detection of multiple miRNAs in pancreatic carcinoma, ACS Appl. Mater. Interfaces 9 (2017) 24118–24125.
[30] F. Jin, D. Xu, A fluorescent microarray platform based on catalytic hairpin assembly for microRNAs detection, Anal. Chim. Acta 1173 (2021), 338666.
[31] A. Afzalinia, M. Mirzaee, Ultrasensitive fluorescent miRNA biosensor based on a "sandwich" oligonucleotide hybridization and fluorescence resonance energy transfer process using an Ln(III)-MOF and Ag nanoparticles for early cancer diagnosis: application of central composite design, ACS Appl. Mater. Interfaces 12 (2020) 16076–16087.
[32] Y.-S. Borghei, M. Hosseini, M.R. Ganjali, S. Hosseinkhani, Label-free fluorescent detection of microRNA-155 based on synthesis of hairpin DNA-templated copper nanoclusters by etching (top-down approach), Sensor. Actuator. B Chem. 248 (2017) 133–139.
[33] Y. Jiang, Q. Li, Y. Xu, W. Bai, X. Yang, S. Li, et al., Electrochemiluminescent emission potential tunable Cu–Zn–In–S/ZnS nanocrystals for multiplex microRNAs potential-resolved detection, Biosens. Bioelectron. 201 (2022), 113980.
[34] F. Wang, C. Fu, C. Huang, N. Li, Y. Wang, S. Ge, et al., Paper-based closed Au-Bipolar electrode electrochemiluminescence sensing platform for the detection of miRNA-155, Biosens. Bioelectron. 150 (2020), 111917.
[35] F. Wang, Y. Liu, C. Fu, N. Li, M. Du, L. Zhang, et al., Paper-based bipolar electrode electrochemiluminescence platform for detection of multiple miRNAs, Anal. Chem. 93 (2021) 1702–1708.
[36] P. Zhang, Z. Lin, Y. Zhuo, R. Yuan, Y. Chai, Dual microRNAs-fueled DNA nanogears: a case of regenerated strategy for multiple electrochemiluminescence detection of microRNAs with single luminophore, Anal. Chem. 89 (2017) 1338–1345.
[37] Y. Chang, Z. Wu, Q. Sun, Y. Zhuo, Y. Chai, R. Yuan, Simply constructed and highly efficient classified cargo-discharge DNA robot: a DNA walking nanomachine platform for ultrasensitive multiplexed sensing, Anal. Chem. 91 (2019) 8123–8128.